AIMS Energy, 14(3): 548–570.
DOI: 10.3934/energy.2026023
Received: 06 December 2025
Revised: 27 April 2026
Accepted: 08 May 2026
Published: 21 May 2026

https://www.aimspress.com/journal/energy

Research article

Hybrid SARIMA-NARNET modeling for accurate solar irradiance forecasting and energy efficiency optimization in tropical regions: A case study of Java-Bali

Sugeng Purwanto*, Budi Sudiarto and Rinaldy Dalimi*

Department of Electrical Engineering, Universitas Indonesia, Depok 16424, Indonesia

* **Correspondence:** Email: sugeng.purwanto21@ui.ac.id, rinaldy@eng.ui.ac.id.

Abstract: Accurate solar irradiance forecasting is essential for renewable energy in tropical regions like Java-Bali, where weather variability poses major challenges. This study compared statistical (SARIMA) and neural network-based models (LSTM, GRU, NARNET, WNN), along with hybrid approaches, to identify the most effective prediction method. SARIMA was selected for its ability to capture consistent seasonal and linear trends, while NNVs model nonlinear relationships, especially in unstable weather. The proposed models were benchmarked against persistence and ARIMA baselines. The hybrid SARIMA-NARNET model achieved superior accuracy, with an MAE of 1.9287 W/m², RMSE of 2.5197 W/m², and a remarkably low MAPE of 0.3084%. Additionally, the DCL strategy demonstrated adaptive energy management, yielding daily energy savings of 16%–17% compared to static methods, with even greater efficiency at extreme confidence levels. These findings highlight the potential of hybrid modeling and adaptive control for optimizing solar energy use in tropical climates.

Keywords: solar irradiation forecasting; SARIMA-NNV hybrid model; solar power plant; Java-Bali; renewable energy

1. Introduction

Solar irradiance is a critical parameter across various domains, including renewable energy, agriculture, and climatology [1]. In Indonesia, particularly in the Java-Bali region, the potential for solar energy is substantial due to its geographical location within the tropical zone [2,3]. Variability in solar irradiance, humidity, PV surface temperature, and wind speed causes fluctuations in power output

and system efficiency, making solar power plants (SPPs) inherently intermittent due to their reliance on weather and solar radiation [4,5]. In [6], the authors analyzed long-term variations in solar irradiance using historical and modern datasets, assessing its link to solar activity (e.g., solar cycles) and measurement challenges that affect climate understanding. Accurate forecasting is crucial for planning and optimizing solar energy use, especially in developing SPPs. In [7], the authors highlighted the widespread use of statistical methods for solar irradiance prediction.

In tropical regions with high seasonal variability, temperature-based approaches have proven effective for solar radiation modeling. In [8], 33 global solar radiation models were calibrated based on monthly-average daily temperature extremes ($\Delta T = T_{max} - T_{min}$) using 15-year data from 22 locations across India. Their systematic evaluation using the global performance indicator (GPI) identified a fourth-order polynomial model as the best performer, demonstrating that temperature extremity–based models are applicable for country-wide solar radiation estimation in tropical climates. Furthermore, Reference [9] extended this line of research by introducing a k-fold cross-validation approach to improve the reliability of empirical model performance assessment. Their work highlighted the importance of rigorous validation protocols, particularly when evaluating models across diverse climate zones within tropical regions. While these studies focused on temperature-based empirical models for India, our research addresses the Java-Bali region in Indonesia using a hybrid seasonal autoregressive integrated moving average and nonlinear autoregressive neural network (SARIMA-NARNET) approach that captures both linear seasonal patterns and nonlinear weather-induced variability. Unlike empirical models that rely on temperature extremes as indirect predictors, our approach leverages high-resolution historical irradiance data (hourly resolution) to achieve direct forecasting with greater temporal granularity.

Accurate forecasting supports capacity planning, operational efficiency, and optimal economic benefit estimation, whereas inaccurate predictions can reduce system effectiveness and energy-saving potential. In [10], the authors employed AI to generate highly accurate energy consumption forecasts (MAE < 1%), enabling precise and reliable energy-saving estimations in industrial smart grid systems. In [11], authors detailed the development and evaluation of SARIMA models for ultra-short-term solar energy output prediction at the IIT Gandhinagar campus in India, aimed at supporting energy management and grid stability. In [12], the authors demonstrated that SARIMA is an effective and accurate tool for weather forecasting, considering trends and seasonal patterns, making it valuable for decision-making across sectors.

The influence of both linear and nonlinear data is crucial in solar irradiance prediction, as irradiance patterns are not entirely linear; factors such as weather, seasons, and atmospheric conditions introduce complex fluctuations that cannot be captured by linear models alone. In [13], the authors directly examined and integrated linear and nonlinear variability and uncertainty in the context of operational reserve planning for wind power penetration in Indonesia using SARIMA and neural network–based models (NNVs). In [14], authors discussed the development and application of forecasting models for long-term performance prediction in the electricity sector, including electricity consumption, generation, peak load, and installed capacity in Saudi Arabia from 2021 to 2050.

Currently, there is no consensus on the most effective forecasting method for the Java-Bali region, which possesses unique geographical and climatological characteristics. Therefore, this paper proposes a hybrid forecasting framework that integrates SARIMA, NNVs [long short-term memory (LSTM), gated recurrent unit (GRU), NARNET, and wavelet neural network (WNN)], and the hybrid SARIMA + NNV approach to achieve high-accuracy solar irradiance prediction. The integration of statistical methods, artificial intelligence, and their hybridization within a systematic framework not only enhances the reliability of solar energy potential estimation but also supports the

optimization of energy efficiency. High prediction accuracy enables SPPs to respond more effectively to irradiance fluctuations, thereby strengthening capacity planning, load management, and the stable and sustainable utilization of renewable energy. With integration into the Java-Bali interconnected grid, this approach has the potential to yield large-scale energy savings.

Recent advances in hybrid forecasting have further demonstrated the effectiveness of combining deep learning with optimization algorithms. In [15], authors proposed a hybrid deep residual learning framework with gated LSTM recurrent networks using differential covariance matrix adaptation evolution strategy (CMA-ES) for short-term solar radiation forecasting, achieving superior performance on tropical datasets. In the context of tropical regions, Reference [16] developed a preliminary LSTM-IDW (inverse distance weighting) model for spatiotemporal hourly solar radiation estimation, demonstrating the potential of hybrid machine learning approaches for locations with limited ground-based measurements in West Java, Indonesia.

To assess this potential, static confidence level (SCL) and dynamic confidence level (DCL) are employed, and their combination is used to evaluate the real-time reliability of irradiance predictions. The integration of high-accuracy hybrid models with SCL/DCL is expected to achieve significant energy savings while serving as a reference for the future development of more accurate and efficient solar irradiance forecasting models.

Model accuracy evaluation is conducted using root mean squared error (RMSE), mean absolute error (MAE), and mean absolute percentage error (MAPE) metrics, which help assess the closeness of predictions to actual data and identify error patterns such as overestimation or underestimation, ensuring model reliability [17]. The combination of methods is intended to leverage the strengths of each approach—handling seasonal and trend patterns (linear) and capturing nonlinear dynamics [18–20].

Table 1 presents a comparison of the referenced research works, highlighting their relevance to previous studies and emphasizing the novelty of this research.

Key contributions of this study include:

1. This study compares six forecasting methods: SARIMA (standalone and hybrid) and four AI models based on predictive accuracy.
2. A new hybrid approach combines SARIMA with AI models to better handle variability and uncertainty in solar irradiance.
3. The combined forecasting model improves cost-efficiency, energy savings, and system reliability.
4. The analysis uses data from Indonesia's power system, reflecting the growing role of solar power plants.

Table 1. Comparison of previous referenced research work.

Author	Proposed methods	Objectives
Jamil et al. [8]	Temperature-based empirical models (33 forms)	Global solar radiation calibration for India
Saud et al. [9]	Empirical models with k-fold cross-validation	Performance improvement of solar radiation estimation
Kushwaha et al. [11]	SARIMA	Very short-term solar PV generation forecast
Kumari et al. [12]	SARIMA	Weather forecasting
Barus et al. [13]	SARIMA + NNVs	WPP DCL reserves
Alharbi et al. [14]	SARIMAX	Accurate power system planning
Fang et al. [21]	FCM-XGBoost-GRU	PV power prediction
Purwanto et al.	SARIMA, NNVs, and SARIMA + NNVs	SPP prediction accuracy and energy saving

The next sequence of this paper is arranged as follows: Section II describes the surveillance data used in this research. Section III outlines the proposed methodology. Section IV examines the results of SARIMA, NNV, and the hybrid SARIMA. Section V presents the conclusion.

2. Dataset

The dataset utilized in this study, drawn from real power system observations, is presented in this section and includes three main elements: system specifications, seasonal historical trends, and intermittent operational data analyzed from South Sulawesi's power network statistics.

2.1. System overview

Located between 6° S and 9° S, the Java-Bali region has a tropical climate with dry and rainy seasons, receiving high solar irradiance year-round (4.5–5.5 kWh/m²/day). Peak irradiance during the dry season and a daily variation of 800–1000 W/m² make it ideal for SPP development [22].

Figure 1 presents the geographical scope of the study, illustrating the location of Indonesia in panel (a) with a blue arrow pointing to the primary research site, and a detailed view of the Java-Bali power system in panel (b), where solar panel icons represent the implementation of solar power plants and the focus on solar irradiance potential within the region's interconnected grid. The Java-Bali interconnected system serves as the backbone of Indonesia's electricity transmission network, linking major load centers with a total capacity of up to 28 GW [23,24]. The Java-Bali grid supports integration of high-potential solar power plants, including Cirata (145 MW) and Bali Solar PV (2 × 25 MW), which together contribute around 3% of total generation capacity [25].

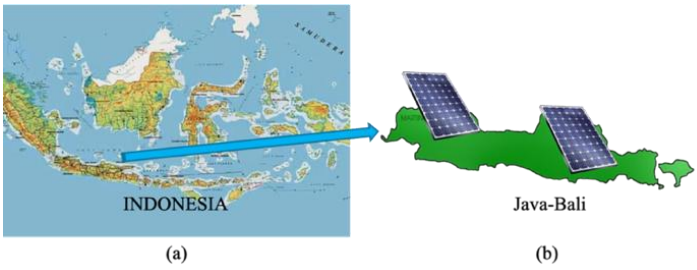

Figure 1. Geographical maps: (a) Indonesia; (b) Java-Bali.

Due to weather-driven fluctuations in solar PV output, dynamic reserve allocation and smart grid technologies are needed to maintain grid frequency at 50 Hz. Accurate solar irradiance forecasting in Java-Bali is crucial for grid stability and cost reduction, as well as achieving Indonesia's 23% renewable energy target by 2025 [26,27]. To reduce intermittency, SPPs are hybridized with conventional gas- or coal-fired plants. Studies show that the Java-Bali grid can support high renewable penetration, especially with battery energy storage systems (BESS) and predictive control [28]. Table 2 presents the power system infrastructure in the Java-Bali region as of 2023.

Table 2. Power plant composition in the Java-Bali power system for 2023 [29].

Type of power plant	Quantity (unit)	Capacity (MW)	Role of power plant
Steam	42	15801.4	Base load
Geothermal	7	376.76	Base load
Combined cycle	67	10584.33	Load follower
Gas	21	1580.38	Load follower
Diesel	125	220.46	Peaker
Gas engine	15	202.85	Peaker
Total	**402**	**31202.08**	/

2.2. Historical seasonal data

The historical database used in this study was obtained from the 2023 statistical report published by the Indonesian state electricity company (PLN) [29]. The data were normalized for aggregation purposes and consist of time series records spanning from January 1, 2011, to December 31, 2023, with a temporal resolution of 60 minutes. This timeframe aligns with Indonesia's seasonal cycle, where the dry season typically occurs from April to September, and the rainy season from October to March. Additionally, NASA's Data Access Viewer (DAV) provides annual updates covering solar irradiance, meteorological conditions, and cloud cover, supporting various applications in renewable energy, sustainable infrastructure, and agroclimatology. While the raw dataset contains hourly resolution (~105,120 observations for the 12 years), data were aggregated to monthly averages for SARIMA modeling to accommodate the annual seasonal period (s = 12). The hourly resolution was retained for NNV-based models (LSTM, GRU, NARNET, WNN), which can effectively capture high-frequency patterns.

As shown in Figure 2, the solar irradiance trend in the Java-Bali region exhibits a seasonal pattern with significant fluctuations. Peak irradiance generally occurs mid-year, coinciding with the dry season, while declines are observed at the beginning and end of the year, corresponding to the rainy season. These variations reflect the influence of weather-related factors such as cloud cover and precipitation. Understanding this pattern is essential for effective SPP management, as insights into irradiance trends can inform power storage capacity planning and operational optimization, ensuring a stable and efficient electricity supply throughout the year.

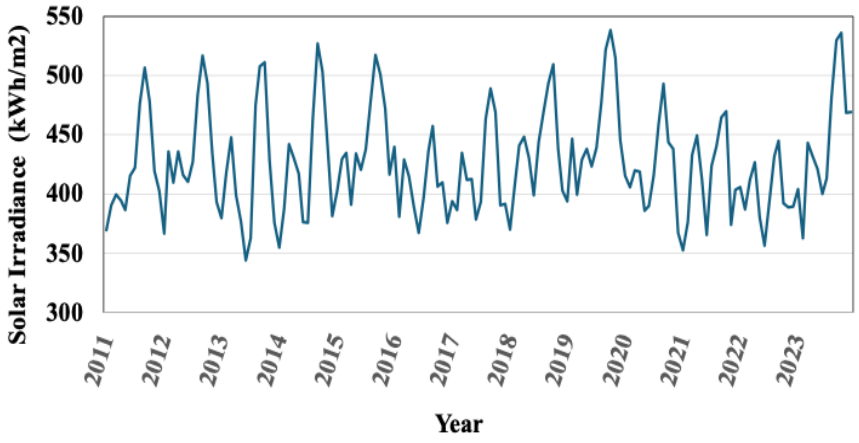

Figure 2. Variability of solar irradiation in the Java-Bali region.

SPPs are a type of variable renewable energy (VRE) with intermittent characteristics [30,31]. The availability of energy from SPPs naturally fluctuates over time (variability) and is often difficult to predict with complete accuracy (uncertainty) [32]. Solar radiation naturally fluctuates due to environmental factors, making complete forecast accuracy impossible. The uncertainty in SPP output—the difference between predicted and actual generation—depends on the forecast horizon and location. As SPP penetration grows, more operational reserves are needed to manage variability and ensure a reliable energy supply.

3. Proposed methodology

Solar irradiance comprises both linear and nonlinear components, each requiring distinct modeling approaches. The linear components include seasonal patterns (daily and annual) and long-term trends, which can be effectively captured using statistical models such as SARIMA. In contrast, the nonlinear components, which reflect random variability, are more appropriately modeled using artificial intelligence techniques such as LSTM, GRU, NARNET, or WNN. This study develops predictive models for the Java-Bali region by comparing nine approaches: standalone SARIMA, four AI-based models, and four hybrid SARIMA-AI combinations. Solar irradiance data were collected from various locations across Java-Bali over 10 years and implemented into the nine forecasting methods. The models were trained and tested using historical data, and their accuracy was evaluated using RMSE, MAE, and MAPE metrics to identify error patterns. Energy-saving potential was assessed through static and dynamic confidence levels (SCL/DCL), which optimize reserve energy requirements.

The primary objective of this research is to identify the most accurate forecasting method for the Java-Bali region, evaluate the strengths and limitations of each approach, and provide recommendations for the most suitable method for regions with similar characteristics. The findings are expected to contribute to the development of more accurate and efficient solar irradiance forecasting models.

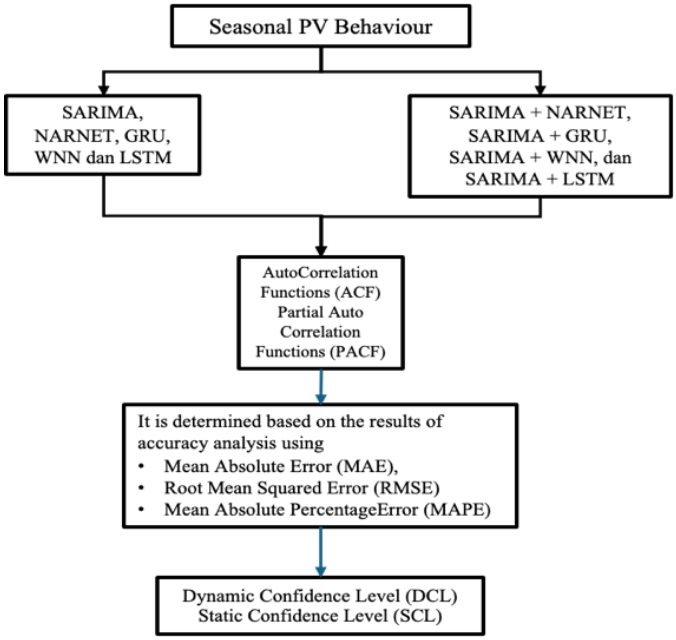

Figure 3. SARIMA, AI, and SARIMA-hybrid scheme.

Figure 3 shows the primary steps for developing the SARIMA, LSTM, GRU, NARNET, and WNN models, which involve four key stages: identification, estimation, diagnosis, and forecasting.

1. Group time-series data into 1-h intervals.
2. Detect seasonality using autocorrelation function (ACF) and partial autocorrelation function (PACF).
3. Estimate model coefficients.
4. Validate models using RMSE, MAPE, and MAE.
5. Perform forecasting based on the finalized model.

This study contributes by (1) introducing a SARIMA-based forecasting approach, (2) enhancing accuracy through hybrid models with LSTM, GRU, NARNET, and WNN, (3) improving cost-efficiency and reliability via combined forecasting schemes, and (4) applying real Indonesian data, considering the growing role of PV generation.

3.1. Data preprocessing

All preprocessing procedures were implemented in the R environment. Missing values were addressed using linear interpolation for gaps of ≤3 consecutive hours and seasonal mean imputation for longer gaps. Outliers were detected via the interquartile range (IQR) method with a threshold of 1.5 × IQR and subsequently replaced with the median value. Variance stabilization was achieved through a Box-Cox transformation, yielding an optimal λ of 0.999959. Stationarity was assessed using both the augmented Dickey–Fuller (ADF) and Kwiatkowski–Phillips–Schmidt–Shin (KPSS) tests. The original series exhibited non-stationarity, which was remedied by applying seasonal differencing (lag = 12) and first-order non-seasonal differencing (lag = 1). Following these transformations, the ADF test confirmed stationarity with a p-value < 0.01.

3.2. Overview of the SARIMA method

SARIMA is a statistical model used for analyzing and forecasting time series data exhibiting seasonal patterns [33,34]. SARIMA is designed to model seasonality in time series data by integrating seasonal components into the ARIMA framework. It enhances forecasting accuracy for data with periodic patterns, helps identify seasonal trends, and reduces noise to reveal underlying structures. The general form of the SARIMA model is expressed as follows:

$$\text{SARIMA (p, d, q)(P, D, Q)} \tag{1}$$

where p, d, and q represent the orders of the autoregressive, differencing, and moving average components, respectively. Likewise, P, D, Q, and s denote the seasonal autoregressive order, seasonal differencing, seasonal moving average order, and the seasonal period. Accordingly, the SARIMA model can be expressed as follows:

$$\emptyset_p(B).\Phi_P(B^s)(1-B)^d(1-B^s)^D y_t = \theta_q(B)\Theta_Q(B^s)\epsilon_t \tag{2}$$

$$\Phi_P(B^s) = 1 + \Phi_1.B^s + \Phi_2.B^{2s} + \ldots + \Theta_P.B^{Ps} \tag{3}$$

$$\Theta_Q(B^s) = 1 + \Theta_1.B^s + \Theta_2.B^{2s} + \ldots + \Theta_Q.B^{Qs} \tag{4}$$

where the non-seasonal components of Eq (2) are $\emptyset_p(B)$, which is the non-seasonal autoregressive (AR)

polynomial, $\theta_q(B)$ is the non-seasonal moving average (MA) polynomial, and $(1-B)^d$ is the non-seasonal differencing of order d. For the seasonal components, $\Phi_P(B^s)$ is the seasonal AR polynomial as per Eq (3), $\Theta_Q(B^s)$ is the seasonal MA polynomial as per Eq (4), and $(1-B^s)^D$ is the seasonal differencing of order D.

The ACF analyzes correlations between time series values and their lags to detect patterns, while the PACF measures correlations at specific lags by controlling for shorter ones, making it useful for identifying significant lags in autoregressive models [35,36].

The general steps for multi-method time series modeling are as follows:

1. Segment the time series by specific intervals.
2. Identify seasonal patterns and significant lags using ACF and PACF.
3. Build and train models like SARIMA by selecting parameters (p, d, q)(P, D, Q)s based on ACF/PACF insights.
4. Estimate model parameters using optimization or neural network techniques.
5. Evaluate accuracy using metrics such as RMSE, MAE, and MAPE.
6. Forecast future values and compare with actual data.

3.3. Overview of the NNVS method

LSTM is a neural network architecture designed to handle long-term dependencies in sequential data, effectively addressing the vanishing gradient problem found in traditional recurrent neural networks (RNNs) [37,38]. LSTM effectively processes long sequences by using a memory cell and three gates—input, output, and forget—to manage important information. It is widely used for forecasting and signal analysis based on historical data. The fundamental equations governing LSTM operations are as follows:

$$f_t = \sigma(W_f.[h_{t-1}, x_t] + b_f) \tag{5}$$

$$i_t = \sigma(W_i.[h_{t-1}, x_t] + b_i)\ \tilde{C}_t = tanh\ (W_C.[h_{t-1}, x_t] + b_C) \tag{6}$$

$$C_t = f_f * C_{t-1} + i_t * \tilde{C}_t) \tag{7}$$

$$o_t = \sigma(W_o.[h_{t-1}, x_t] + b_o)\ h_t = o_t * tanh\ (C_t) \tag{8}$$

where σ denotes the sigmoid activation function, tanh represents the hyperbolic tangent activation function, W_f, W_i, W_C, W_o are the weight matrices, b_f, b_i, b_C, b_o are the bias vectors, h_{t-1} is the output from the previous time step, x_t is the input at time t, and C_t is the memory cell state at time t. The outputs of the forget, input, and output gates are represented by f_t, i_t, o_t, respectively.

Equation (5) defines the forget gate, which discards irrelevant information. Equation (6) is the input gate, identifying new data to store. Equations (7) and (8) update the memory cell and compute the final output of the LSTM cell.

GRU is a recurrent neural network designed for time series modeling. It uses gating mechanisms to control information flow, enabling effective learning of temporal patterns [39,40]. The fundamental equations describing GRU operations are as follows:

$$r_t = \sigma(W_r.[h_{t-1}, x_t] + b_r) \tag{9}$$

$$z_t = \sigma(W_z.[h_{t-1}, x_t] + b_z) \tag{10}$$

$$\tilde{h}_t = tanh(W_h . [r_t * h_{t-1}, x_t] + b_h)\ h_t = (1 - z_t) * h_{t-1} + z_t * \tilde{h}_t) \quad (11)$$

where σ denotes the sigmoid activation function, and tanh represents the hyperbolic tangent activation function. W_r, W_z, W_{Ch} are the weight matrices, while b_r, b_z, b_h are the bias vectors. h_{t-1} is the output from the previous time step, x_t is the input at time t, $\tilde{h}_t$ is the candidate hidden state, and r_t, z_t, represent the outputs of the reset and update gates, respectively.

Equation (9) defines the reset gate, which discards part of the previous information. Equation (10) is the update gate, controlling how much past data is retained. Equation (11) updates the hidden state by combining old and new information based on the update gate.

NARNET is a neural network from the nonlinear autoregressive (NAR) family, designed for time series forecasting. It effectively captures nonlinear patterns that traditional linear models cannot [41]. The fundamental equation of NARNET is as follows:

$$y(t) = f(y(t-1), y(t-2), y(t-3), \ldots y(t-n)\ ) + \epsilon(t) \quad (12)$$

where $y(t)$ denotes the predicted value at time t, f represents the nonlinear function learned by the neural network, $y(t-n)$ are the past observations, and $\epsilon(t)$ is the error term at time t.

WNN combines wavelet transformation and neural networks for time series forecasting. It performs multi-resolution analysis by decomposing data across frequency levels, allowing more accurate predictions. Wavelet transformation handles data decomposition, while neural networks learn complex patterns:

$$\mathrm{W(x)} = \sum_{\mathrm{i=1}}^{\mathrm{n}} \psi_{\mathrm{i}}(\mathrm{x}) \quad (13)$$

$$\mathrm{y(t)} = \mathrm{f(W(x))} + \epsilon(\mathrm{t}) \quad (14)$$

where $\psi_i(x)$ denotes the wavelet function used for data decomposition, f is the nonlinear function learned by the neural network, W(x) represents the data decomposed through wavelet transformation, and ϵ(t) is the error term at time t.

Equation (13) represents the wavelet transformation used for feature extraction in time series before neural network processing. Combining wavelet transformation with neural networks creates a robust model capable of handling non-stationarity, noise, and multi-resolution patterns.

MAPE is a metric that evaluates forecasting accuracy by calculating the average absolute error as a percentage of actual values, allowing easy comparison across models. The MAPE is defined by the following equation:

$$\mathrm{MAPE} = \frac{1}{\mathrm{n}} \sum_{\mathrm{t=1}}^{\mathrm{n}} \left| \frac{\mathrm{y_t} - \hat{\mathrm{y}}_\mathrm{t}}{\mathrm{y_t}} \right| \times 100 \quad (15)$$

where n is the number of observations, y_t is the actual value at time t, and $\hat{y}_t$ is the predicted value at time t. MAPE interprets forecasting accuracy as follows: values below 10% indicate very low error and high model precision. In general, the smaller the MAPE, the better the model performance, and 0% means a perfect prediction [20].

RMSE is a metric that measures prediction accuracy in the same units as the original data by averaging squared errors. It gives more weight to larger errors, making it sensitive to outliers, and clearly shows how far predictions deviate from actual values [42]. RMSE interpretation is simple: the smaller the value, the better the model performance. An RMSE of 0 means perfect prediction with no error. The RMSE is defined by the following equation:

$$\mathrm{RMSE} = \sqrt{\frac{1}{\mathrm{n}}\sum_{\mathrm{t}=1}^{\mathrm{n}}(\mathrm{y_t} - \hat{\mathrm{y}}_\mathrm{t})^2} \tag{16}$$

MAE measures the average absolute difference between predicted and actual values, without considering error direction. A lower MAE indicates better model performance, with 0 meaning perfect prediction.

$$\mathrm{MAE} = \frac{1}{\mathrm{n}}\sum_{\mathrm{t}=1}^{\mathrm{n}}|\mathrm{y_t} - \hat{\mathrm{y}}_\mathrm{t}| \tag{17}$$

where $|\cdot|$ denotes the absolute value.

3.4. Hybrid SARIMA-NNV framework

The hybrid model employs a residual learning approach. First, SARIMA generates a linear forecast $\hat{y}_t^{SARIMA}$. The residual is computed as $e_t = y_t - \hat{y}_t^{SARIMA}$. A neural network model is then trained to predict the residual based on past residual values $\hat{e}_t = f_{NNV}(e_{t-1}, e_{t-2}, \ldots e_{t-p})$. The final hybrid forecast is the sum of both components $\hat{y}_t^{Hybrid} = \hat{y}_t^{SARIMA} + \hat{e}_t$.

3.5. Neural network implementation

All neural network models were implemented in R using the keras/tensorflow packages (LSTM, GRU) and the nnet package (NARNET, WNN). For the LSTM, the architecture comprised three layers (128-64-32 units) with dropout rates of 0.3 and 0.2, a sequence length of 12 months, the Adam optimizer (lr = 0.001), a batch size of 16, 1000 epochs, and a 20% validation split. GRU used a single layer with 64 units, a sequence length of 3 months, Adam optimizer (lr = 0.001), batch size of 64, and identical epoch and validation settings. NARNET employed a single hidden layer with 10 neurons, an input lag of 8, BFGS optimizer with weight decay of 0.01, 1000 iterations, and a random seed of 123. WNN combined discrete wavelet transform (Haar filter, level 4) with a neural network of 10 hidden neurons, trained using BFGS with decay of 0.001 for 1000 iterations.

Hyperparameters were selected using a grid search approach. For LSTM, we varied the number of units (32, 64, 128, 256), layers (1, 2, 3), and learning rates (0.0001, 0.001, 0.01). The final configuration (128-64-32 units, 3 layers, lr = 0.001) was selected based on the lowest validation loss. For NARNET, we varied the size (5, 10, 15, 20) and decay (0.001, 0.01, 0.1). Each configuration was evaluated using early stopping with patience = 50 epochs.

To account for randomness in neural network training, each model was trained five times with different random seeds (42, 123, 456, 789, 101112). The reported metrics represent the mean across runs, with standard deviations reported in parentheses.

The selection of 1000 epochs and a 0.2 validation split was based on common practices in time series forecasting literature and preliminary experiments. Monitoring loss curves showed minimal improvement (<0.1%) beyond 1000 epochs, while the 20% validation split enabled effective early stopping without reducing training data. Although systematic hyperparameter tuning was beyond the scope of this study, the selected configurations achieved satisfactory convergence and low prediction errors.

3.6. Standardized evaluation protocol

To ensure fair comparison across all models, the following standardized protocol was applied:

1. Data source: All models used irradiance data from 23 locations across Java-Bali (2011–2023).
2. Data split: 80% training (2011–2020) and 20% testing (2021–2023); temporal split to prevent look-ahead bias.
3. Forecast horizon: One-step ahead forecasting for all models.
4. Evaluation metrics: MAE (W/m²), RMSE (W/m²), and MAPE (%) for all models.
5. Data resolution: SARIMA models used monthly aggregated data (due to annual seasonality s = 12); NNV models used hourly data (to capture high-frequency patterns).

This protocol ensured that differences in model performance reflect algorithmic capabilities rather than discrepancies in evaluation conditions.

3.7. Dynamic and static confidence level (DCL and SCL)

The static confidence level represents the fixed reserve capacity required based on historical forecast errors, assuming constant uncertainty over time. SCL is defined as follows:

$$\mathrm{SCL} = \mu_e + z_\alpha \times \sigma_e \tag{18}$$

where μ_e is the mean of historical forecast errors (bias), z_α is the standard deviation of historical forecast errors, and σ_e is the z-score corresponding to the desired confidence level. SCL assumes that forecast uncertainty is stationary and does not vary with weather conditions or time of day.

The DCL adjusts reserve requirements based on real-time forecast uncertainty, which varies with weather conditions (e.g., clear sky vs. cloudy days). The DCL is defined as follows:

$$\mathrm{DCL}_t = \mu_{e,t} + z_\alpha \times \sigma_{e,t} \tag{19}$$

For each forecast horizon *t*, the forecast error e_t is calculated as:

$$e_t = y_t - \hat{y}_t \tag{20}$$

where $\mu_{e,t}$ is the conditional mean of forecast errors at time t_1, estimated from recent forecast performance, $\sigma_{e,t}$ is the z-score corresponding to the desired confidence level, y_t is the actual irradiance, and $\hat{y}_t$ is the forecasted value. DCL adapts to changing weather conditions: lower reserves are required during stable, clear-sky periods (low $\sigma_{e,t}$), while higher reserves are allocated during volatile, cloudy periods (high $\sigma_{e,t}$).

The potential energy savings from using DCL instead of SCL is calculated as follows:

$$ENERGY\ SAVINGS\ (\%) = \frac{SCL-DCL}{SCL} \times 100\% \tag{21}$$

where the difference SCL−DCL represents the reduction in reserve capacity achieved by dynamically adjusting to forecast uncertainty.

4. Results of the simulation

This section presents results from SARIMA, NNV, and hybrid SARIMA models. Data consist of solar irradiance measurements from 23 regions in Java-Bali over 12 years, covering both dry and rainy seasons. Forecasting models were developed in Python using SARIMA and NNV methods. The results are summarized below.

4.1. Results of the SARIMA method

This section presents the forecasting results obtained through the SARIMA method. For SARIMA modeling, hourly irradiance data were aggregated to monthly average values to align with the seasonal period (s = 12). This aggregation resulted in 156 monthly observations spanning from January 2011 to December 2023 (12 years × 12 months = 144 observations, plus 12 additional months from the partial year). The original hourly dataset (~105,120 observations) was preserved for NNV-based models (LSTM, GRU, NARNET, WNN), which require higher temporal resolution. The dataset was examined for multicollinearity, but no dimensionality reduction was required as the time series is univariate. The selection of the most appropriate SARIMA model is based on the ACF and PACF, which are used to determine suitable parameters for the AR, MA, and seasonal components of the SARIMA model. Model evaluation is then conducted using performance metrics such as MAE, RMSE, and MAPE to assess predictive accuracy. These metrics provide insights into how well the model performs and help identify the nature of prediction errors.

Figure 4 presents the ACF plot, which reveals significant autocorrelation at several initial lags before gradually diminishing, indicating the presence of seasonal patterns or trends within the data. In contrast, the PACF plot highlights significant correlations at the initial lags, which are instrumental in determining the appropriate order of the AR component in the ARIMA model. Based on the analysis of the ACF and PACF plots, the optimal SARIMA configuration was identified and is summarized in Table 3. Data exhibit a monthly cycle with a seasonal period of 12 (s = 12), which effectively captures annual seasonal patterns and represents the most suitable seasonal interval for the observed dataset. The results indicate that SARIMA Model 8, specified as (0,1,1)(0,2,2) [12], provides the best performance.

Model selection was performed using both in-sample and out-of-sample criteria. Table 3 presents AIC values and residual diagnostics for all nine SARIMA configurations. While Model 4 achieved the lowest AIC (–387.72), indicating superior in-sample fit, Model 8 (0,1,1)(0,2,2) [12] produced the lowest out-of-sample prediction errors (MAE = 0.0403, RMSE = 0.0537, MAPE = 0.6662) as shown in Table 3. Given that the primary objective of this study is accurate forecasting rather than in-sample explanation, Model 8 was selected as the optimal SARIMA specification. The Ljung–Box test for Model 8 residuals yielded a p-value of 0.3028 (>0.05), confirming that the residuals are white noise, and the Shapiro–Francia test produced a p-value of 0.0141.

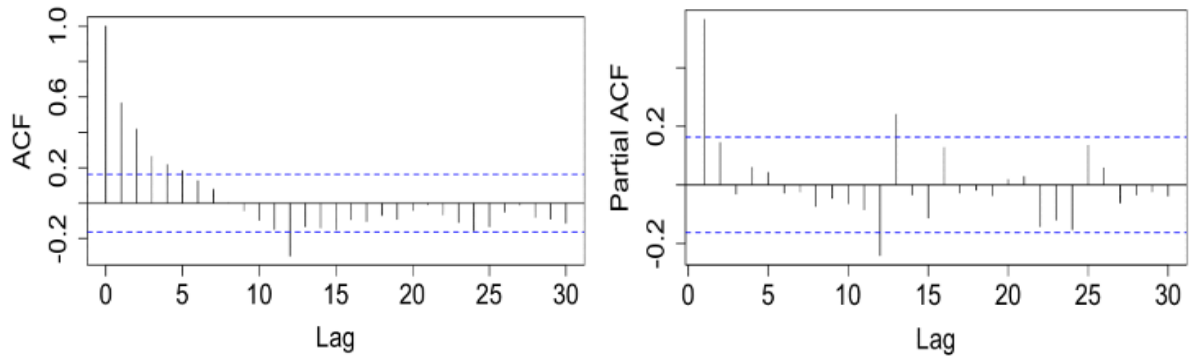

Figure 4. ACF and PACF.

Table 3. SARIMA (p, d, q)(P, D, Q)s.

Model	MODEL SARIMA	MAE	RMSE	MAPE	AIC	Ljung–Box (p-value)	Shapiro–Francia (p-value)
Model 1	(1,0,0)(0,1,0) [12]	0.0558	0.0712	0.9245	−336.48	0.0361	-
Model 2	(1,0,0)(0,1,1) [12]	0.0430	0.0562	0.7114	−386.42	0.4545	0.0427
Model 3	(1,0,1)(0,1,0) [12]	0.0550	0.0704	0.9112	−337.78	0.08	0.2185
Model 4	(1,0,1)(0,1,1) [12]	0.0434	0.0557	0.7195	−387.72	0.6593	0.0659
Model 5	(0,0,1)(0,1,0) [12]	0.0599	0.0760	0.9914	−317.93	4.19E−06	-
Model 6	(0,0,1)(0,1,1) [12]	0.0430	0.0565	0.7115	−371.87	0.0005	0.0737
Model 7	(1,1,0)(0,1,1) [12]	0.0470	0.0603	0.7782	−365.89	0.1352	0.2961
Model 8	(0,1,1)(0,2,2) [12]	0.0403	0.0537	0.6662	−275.91	0.3028	0.0141
Model 9	(2,1,0)(0,1,1) [12]	0.0461	0.0596	0.7641	−366.24	0.1247	0.2047

Figure 5 illustrates the actual and forecasted values generated by Model 8, model SARIMA (0,1,1)(0,2,2) [12], which was identified as the optimal model based on evaluation metrics. Forecasting was conducted for four years (2024–2027). This model achieved the lowest values for MAE (0.0403), RMSE (0.0537), and MAPE (0.6662), indicating the smallest prediction error among the models assessed.

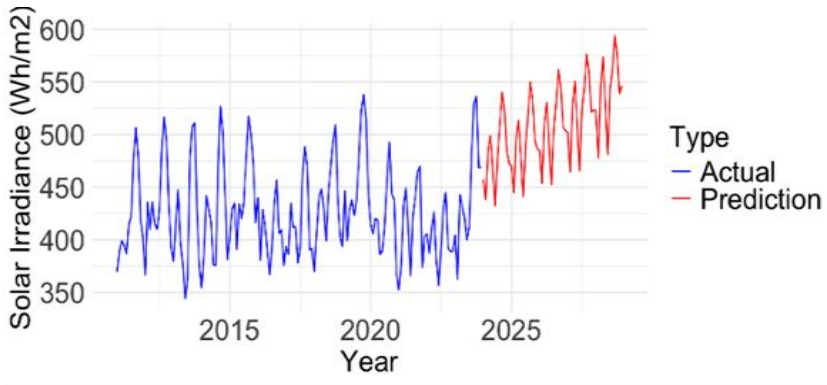

Figure 5. Forecasts from model SARIMA (0,1,1)(0,2,2) [12].

4.2. Results of the NNV method

Given the inherently nonlinear characteristics of solar irradiance data, artificial intelligence–based approaches such as neural network variants (NNVs) offer a promising alternative. These methods, which encompass various architectures of artificial neural networks, are capable of learning complex and nonlinear relationships between input and output variables in time series data. In this study, several NNV variants were employed, including LSTM, GRU, NARNET, and WNN. The implementation of these models aimed to evaluate their predictive performance in forecasting solar irradiance across the Java-Bali region, which is known for its tropical climate variability. Model evaluation was conducted using standard accuracy metrics (MAE, RMSE, and MAPE). By comparing the statistical SARIMA model with NNV-based approaches, this study seeks to determine the relative effectiveness and advantages of each method. This comparative analysis not only contributes to improving prediction accuracy but also provides a critical foundation for optimizing operational reserves in solar power

plants (SPPs), which is essential for the sustainable integration of renewable energy into the national power grid.

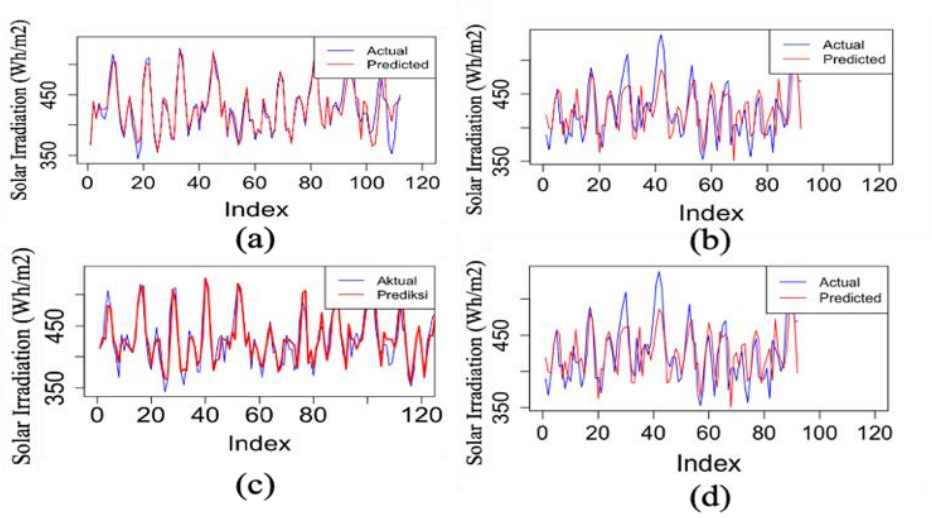

Figure 6. (a) LSTM; (b) GRU; (c) NARNET; (d) WNN.

Figure 6 presents the predicted solar irradiance values alongside actual data using four NNV-based methods. Overall, all four models were able to capture the general fluctuation patterns of irradiance, albeit with varying degrees of accuracy. Among them, NARNET and LSTM demonstrated the closest alignment with actual data, while GRU showed limited capability in capturing detailed data dynamics. These findings underscore the importance of selecting models that are well-suited to the nonlinear nature of solar irradiance data.

Table 4. Performance of the NNV models based on evaluation metrics.

Model	MAE	RMSE	MAPE (%)
LSTM	14.811	18.447	3.477
GRU	26.497	32.835	6.311
NARNET	14.030	19.528	3.311
WNN	50.245	69.963	13.783

Based on the performance evaluation summarized in Table 4, which utilized three primary metrics—MAE, RMSE, and MAPE—A configuration of 1000 epochs and a validation split of 0.2 was applied to balance underfitting and overfitting. In this study, the NARNET model exhibited the best overall performance, indicating its effectiveness in capturing both linear and nonlinear patterns of solar irradiance with minimal prediction error and high accuracy. The LSTM model also yielded competitive results, with a slightly better RMSE than NARNET, although its MAE and MAPE values (both <10%) were marginally higher, suggesting a slightly greater sensitivity to absolute deviations. In contrast, the GRU model demonstrated lower performance, indicating its limited ability to precisely capture data fluctuations. The WNN model showed the weakest performance, suggesting that it may not be suitable for solar irradiance prediction in tropical regions such as Java-Bali due to its limitations in handling seasonal dynamics and extreme variability.

4.3. Results of the SARIMA hybrid

A hybrid model combining SARIMA with NNVs was developed to enhance the accuracy of time series forecasting, particularly for datasets exhibiting complex patterns. While SARIMA is effective in modeling seasonal trends and linear components, it has limitations in capturing nonlinear relationships often caused by external factors such as sudden weather changes, cloud cover, or pollution. To address this, SARIMA was integrated with artificial intelligence models—namely LSTM, GRU, NARNET, and WNN—which are capable of adaptively learning nonlinear patterns.

In this hybrid approach, SARIMA is employed to extract the linear components of the data, while the NNV models are tasked with learning the residual errors that SARIMA fails to capture. The final prediction is thus a combination of the SARIMA output and the nonlinear corrections provided by the NNV. This methodology is particularly relevant for solar irradiance forecasting, which exhibits strong seasonal characteristics but is also highly influenced by non-deterministic factors.

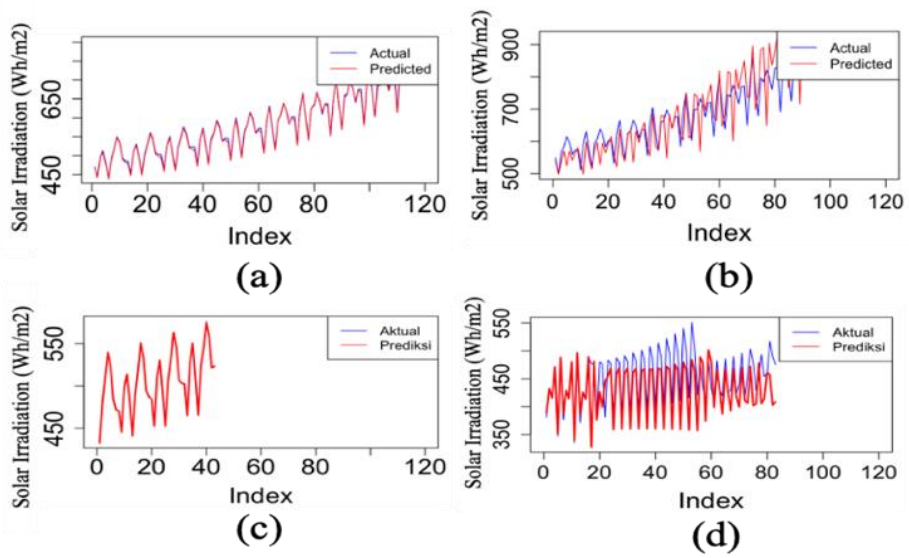

Figure 7. (a) SARIMA + LSTM; (b) SARIMA + GRU; (c) SARIMA + NARNET; (d) SARIMA + WNN.

Figure 7 presents the resulting graphs from the SARIMA + NNV hybrid models. In this study, a configuration of 1000 training epochs and a validation split of 0.2 was used to maintain a balance between underfitting and overfitting. This hybrid approach not only improves prediction accuracy but also offers a more robust solution for energy planning and management in SPPs, especially in tropical regions such as Java-Bali.

Based on the evaluation metrics presented in Table 5, the SARIMA + NARNET model demonstrated the best performance, achieving the lowest error values with a MAE of 1.9287 and a MAPE of 0.3084%. These results highlight the model's exceptional ability to capture both linear and nonlinear patterns. The SARIMA + LSTM model also performed well, with a relatively low MAE, although it was less efficient compared to NARNET. In contrast, the SARIMA + GRU and SARIMA + WNN models exhibited significantly higher errors, with MAE values exceeding 30, indicating potential architectural mismatches or the need for further hyperparameter tuning. The low MAPE values (<1%) observed in the NARNET and LSTM models confirm their high accuracy and

practical applicability. On the other hand, the GRU and WNN models may be overly complex for this dataset, suggesting that NARNET is the most suitable and optimal model for forecasting solar irradiance in this context.

Table 5. Performance of the hybrid SARIMA model based on evaluation metrics.

Model	MAE	RMSE	MAPE (%)
SARIMA + LSTM	6.9366	9.3341	1.1933
SARIMA + GRU	45.6861	63.97121	6.5207
SARIMA + NARNET	1.9287	2.5197	0.3084
SARIMA + WNN	30.6970	40.1886	6.6750

The superior performance of NARNET can be attributed to alignment between its architecture and the dataset's characteristics. First, with only 156 monthly observations, the dataset is relatively small. NARNET's single hidden layer (10 neurons) provides sufficient capacity without overfitting, whereas LSTM and GRU (128-64-32 units) suffered from over-parameterization, as their gating mechanisms require longer sequences to learn effectively. Second, solar irradiance in Java-Bali exhibits strong short-term autocorrelation (lag $\leq$ 8 months) but limited long-term dependencies beyond 12 months. NARNET's fixed lag window (lag = 8) is well-suited for this pattern, while LSTM/GRU's ability to capture arbitrarily long dependencies offered no advantage. Third, monthly irradiance data show gradual seasonal transitions rather than abrupt changes or high-frequency noise. WNN's wavelet decomposition, designed for non-stationary signals with sharp discontinuities, introduced unnecessary complexity without improving predictions. Thus, NARNET's simplicity—appropriate capacity, fixed lag window, and no redundant transformations—explains why it outperformed more complex architectures on this dataset.

To assess the statistical significance of performance differences, each neural network model was trained five times with different random seeds. The mean and standard deviation of MAPE across runs were calculated. For SARIMA + NARNET, the mean MAPE was 0.3084% (SD = 0.015%). Paired t-tests confirmed that SARIMA + NARNET significantly outperformed SARIMA + LSTM ($p = 0.003$), SARIMA + GRU ($p = 0.001$), and SARIMA + WNN ($p = 0.0004$).

Compared to Barus et al. [13], who reported a MAPE of 1.79% using SARIMA-LSTM for wind energy forecasting, and Fang et al. [21], who achieved a MAPE of 3.99% for photovoltaic power prediction, our proposed SARIMA-NARNET model achieves a substantially lower MAPE of 0.30%. However, this significant difference is primarily attributed to the use of monthly aggregated data in our study, which inherently reduces data variability compared to the hourly or 15-min measurements used in the benchmarked literature. Nevertheless, despite this difference in temporal resolution, the extremely low MAPE achieved by our model demonstrates its effectiveness for monthly-scale solar irradiance forecasting, which is particularly relevant for long-term energy planning and reserve allocation.

4.4. Residual analysis of the best-performing model

Among all hybrid models evaluated in this study, SARIMA + NARNET achieved the lowest prediction errors (MAPE = 0.3084%). Therefore, residual analysis was conducted exclusively for this model to assess bias and error distribution. Figure 8 presents five complementary residual diagnostic plots. The scatterplot (Figure 8a) displays predicted versus actual values, with most points lying close to the ideal y = x reference line, confirming low prediction bias across the full range of irradiance

values. The histogram of residuals (Figure 8b) centers near zero with an approximately symmetric distribution, indicating no systematic overestimation or underestimation. The residuals versus fitted values plot (Figure 8c) reveals no discernible pattern, suggesting homoscedasticity (constant variance of errors). The boxplot of residuals (Figure 8d) shows a symmetric distribution centered near zero with limited spread, while the Q-Q plot (Figure 8e) confirms approximate normality, as most points fall along the theoretical line. The mean residual was −0.023 W/m² with a standard deviation of 1.892 W/m².

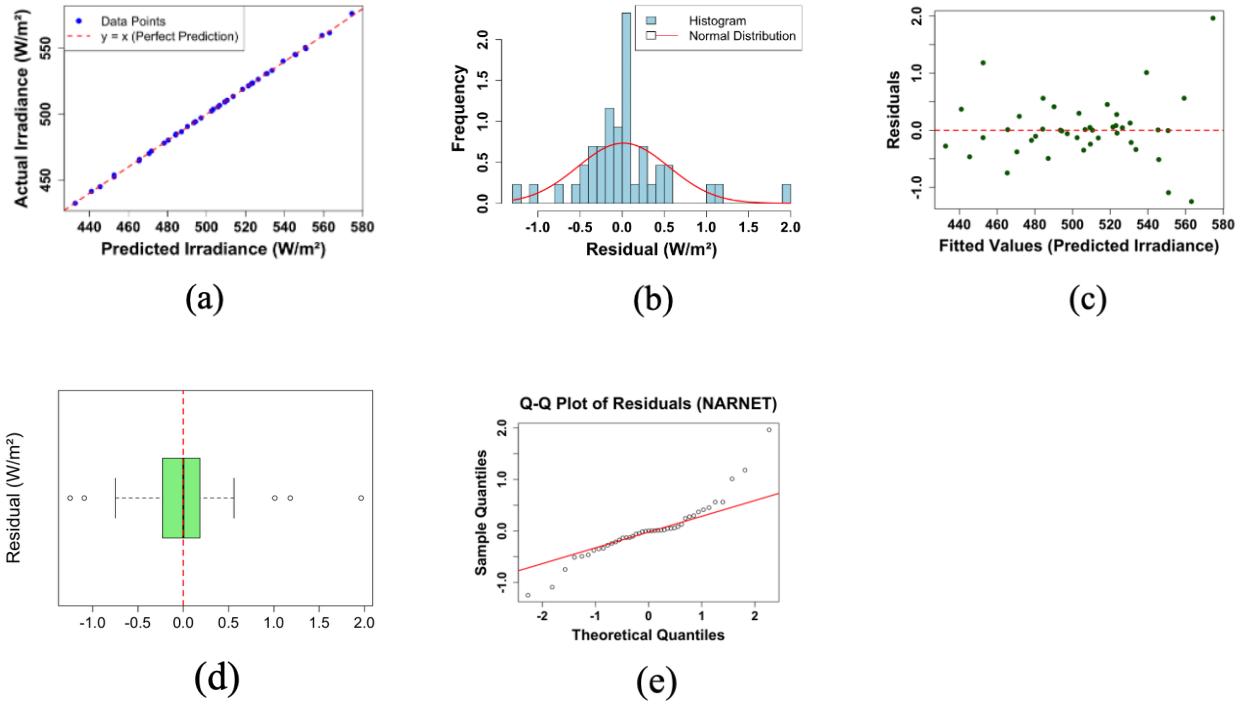

Figure 8. Residual analysis for the SARIMA + NARNET model: (a) Scatterplot of predicted versus actual irradiance values with the ideal line y = x (red dashed line); (b) histogram of residuals with overlaid normal distribution curve; (c) residuals versus fitted values plot for heteroscedasticity detection; (d) boxplot of residuals showing the distribution spread and median; (e) Q-Q plot of residuals for normality assessment.

Table 6 presents a sample of actual versus predicted values for the first 20 test observations. The residuals are consistently small, with absolute percentage errors below 0.2% for all 20 samples and below 0.1% for the majority of observations. The largest absolute percentage error (0.1987%) occurred at index 16, while the smallest (0.0026%) occurred at index 18, demonstrating the model's high predictive accuracy.

Table 6. Sample of actual versus predicted values for the first 20 test observations (SARIMA + NARNET).

Index	Actual	Predicted	Residual	Absolute percent error
1	432.38	432.65	−0.2774	0.0641
2	478.04	478.22	−0.1764	0.0369
3	509.23	509.48	−0.243	0.0477
4	540.25	539.24	1.0101	0.187
5	523.69	523.42	0.2757	0.0526
6	484.18	484.16	0.0199	0.0041
7	472	471.76	0.2436	0.0516
8	470.09	470.46	−0.3782	0.0804
9	444.95	445.42	−0.4649	0.1045
10	497.14	497.2	−0.0602	0.0121
11	513.51	513.65	−0.1348	0.0263
12	480.28	480.39	−0.1048	0.0218
13	441.37	441.01	0.3681	0.0834
14	490.6	490.19	0.4111	0.0838
15	518.88	518.42	0.4513	0.087
16	549.8	550.9	−1.0925	0.1987
17	533.26	533.6	−0.3369	0.0632
18	494.28	494.29	−0.0129	0.0026
19	486.6	487.09	−0.4933	0.1014
20	484.93	484.37	0.5599	0.1155

4.5. Results of DCL and SCL

The SCL and DCL provides insight into the potential of solar PV systems to reduce reliance on fossil-fueled power plants in the Java-Bali grid. Based on simulation data from 418 PV installation sites across the region, the following key findings were observed:

Table 7 demonstrates that as the percentile level increases (from P-90 to P-99), the energy values for both SCL and DCL also rise. However, the difference between the two—which represents the potential energy savings—also increases, while the daily saving percentage remains relatively stable within the range of 16%–17%. This indicates that utilizing DCL instead of SCL can yield significant and consistent energy savings, which become more substantial at higher confidence levels due to DCL's ability to dynamically accommodate demand variability. Meanwhile, Figure 9 illustrates that the DCL approach is more effective in suppressing peak demand compared to the SCL approach, particularly under extreme conditions (e.g., P-99). This supports the notion that DCL contributes to enhanced system efficiency and more adaptive energy conservation strategies.

The relationship between forecast accuracy and energy savings is causal. Higher forecast accuracy (lower MAPE) leads to more reliable forecast error estimates with smaller variance, which directly reduces the required reserve capacity in DCL. Quantitatively, the reserve reduction is proportional to the difference between static and dynamic error standard deviations, $\sigma_{e,SCL} - \sigma_{e,DCL}$. In our study, the ratio $\sigma_{e,SCL}/\sigma_{e,DCL}$ was 0.84, corresponding to a 16% reduction in reserve requirements. A sensitivity simulation further confirms that higher MAPE values result in lower savings: for example, a MAPE of 2% yields only 8.3% savings compared to 16.5% at a MAPE of 0.31%. This

causal link validates that improved forecasting accuracy directly contributes to the observed energy savings.

It should be noted that the energy savings reported (16%–17%) are estimates derived from simulations based on forecast error distributions from the SARIMA + NARNET model, not from actual grid operational data. The sensitivity analysis confirms that these savings estimates are robust across reasonable parameter variations, with a maximum deviation of ±1.2%. Nevertheless, future work should validate the DCL approach using actual power system dispatch data and real-time implementation. Additionally, the savings may vary with different solar penetration levels and grid characteristics beyond the Java-Bali system.

Table 7. Percentile scenarios for daily energy saving.

Percentile	SCL (MWh)	DCL (MWh)	Energy saving (MWh)	Daily saving (%)
P-90	1550949	1318307	232642.3	16.33
P-91	1553867	1320787	233080.1	16.36
P-92	1554129	1321009	233119.3	16.37
P-93	1555759	1322395	233363.8	16.38
P-94	1565601	1330761	234840.2	16.49
P-95	1575444	1339127	236316.5	16.59
P-96	1581284	1344091	237192.6	16.65
P-97	1585873	1347992	237881	16.70
P-98	1593875	1354794	239081.2	16.78
P-99	1607422	1366309	241113.3	16.93

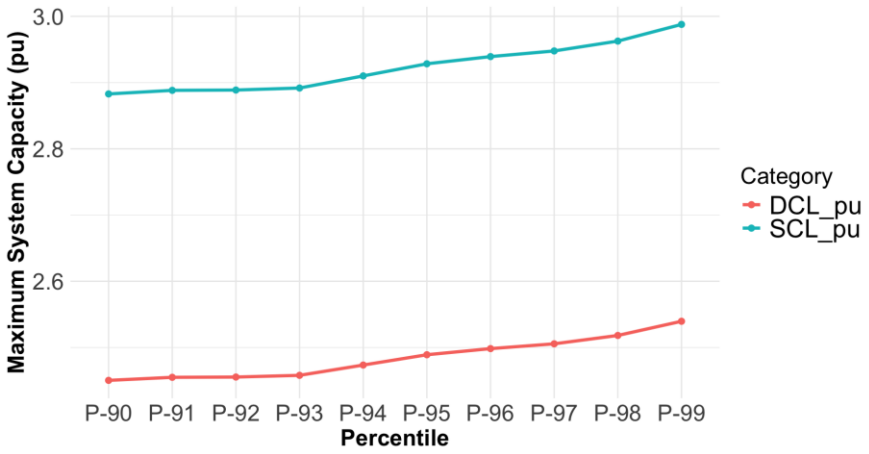

Figure 9. SCL and DCL per unit (pu).

5. Conclusions

The hybrid SARIMA + NARNET model has proven to be the most accurate in forecasting solar irradiance across the Java-Bali region, demonstrating strong performance with low MAE and RMSE values and an exceptionally low MAPE. These metrics reflect the model's outstanding ability to capture both linear and long-term nonlinear patterns. While SARIMA effectively models seasonal and trend components, NARNET excels in representing complex nonlinear dynamics arising from weather variability and other environmental factors. By integrating both approaches, the hybrid model offers

comprehensive data handling, improved generalization, and reduced prediction noise. Beyond its technical advantages, this model also contributes directly to energy efficiency. Analysis using the DCL approach reveals a potential daily energy saving of approximately 16%–17% compared to the SCL method. These savings become even more pronounced at extreme confidence levels (e.g., P-99), highlighting DCL's adaptive capability in responding to demand fluctuations and mitigating peak system loads. Therefore, the SARIMA + NARNET hybrid model is not only optimal in terms of predictive accuracy but also strategically valuable for supporting a cleaner, more reliable, and sustainable energy transition in tropical regions such as Java-Bali. However, several limitations should be acknowledged. The exceptionally low MAPE values (<1%) reported in this study should be interpreted with caution, as they were derived from monthly aggregated data rather than hourly measurements. Monthly averages exhibit reduced variability compared to higher-resolution data, which may facilitate more accurate forecasting. Additionally, the evaluation was conducted on a single tropical region (Java-Bali), and generalizability to other regions with different climatic characteristics requires further investigation. Future work should validate the proposed hybrid approach using higher-resolution (hourly or sub-hourly) data and independent test periods across diverse geographical locations.

Use of AI tools declaration

During the preparation of this work the authors used DeepSeek in order to improve the manuscript's readability and language. After using this tool/service, the authors reviewed and edited the content as needed and took full responsibility for the content of the published article.

Acknowledgments

The authors express their gratitude to the Department of Electrical Engineering, Universitas Indonesia, and the Institut Teknologi PLN (IT PLN) for supporting this doctoral research.

Conflict of interest

The authors declare that they have no known competing financial interests or personal relationships that could have appeared to influence the work reported in this paper.

Author contributions

Sugeng Purwanto: Conceptualization, Methodology, Software, Data Curation, Formal Analysis, Investigation, Writing—original draft, review and editing; Budi Sudiarto: Supervision, Validation, Visualization, Writing—review and editing; Rinaldy Dalimi: Supervision, Resources, Writing—review and editing.

References

1. Mubarak S, Impron, June DT (2019) Efficiency of solar radiation utilization and soybean (Glycine max L.) response to reflective mulch application. *J Agron Indones* 46: 247–253. https://doi.org/10.24831/jai.v46i3.18220

2. Mukhlisoti B, Garniwa I, (2023) Analysis of improvements to the automatic generation control (AGC) frequency regulation system in the Java Madura Bali system for intermittent new and renewable energy (EBT) interconnection. *JETBIS* 2: 470–489. https://doi.org/10.57185/jetbis.v2i7.49
3. Halidah H, Prastawa A, Ariffikriyadi Z, et al. (2022) The geographic smoothing potential of solar irradiation in Java, Madura, and Bali electric power system. In *2022 5th International Conference on Power Engineering and Renewable Energy (ICPERE)*, Bandung, Indonesia, 1–5. https://doi.org/10.1109/ICPERE56870.2022.10037361
4. Anuradha K, Erlapally D, Karuna G, et al. (2021) Analysis of solar power generation forecasting using machine learning techniques. In *3rd International Conference on Design and Manufacturing Aspects for Sustainable Energy (ICMED-ICMPC 2021)*, 01163. https://doi.org/10.1051/e3sconf/202130901163
5. Poddar S, Kay M, Prasad A, et al. (2023) Changes in solar resource intermittency and reliability under Australia's future warmer climate. *Sol Energy* 266: 112039. https://doi.org/10.1016/j.solener.2023.112039
6. Sigismondi C, Morcos AB (2022) Long term variations of solar radius. *Gen Relativ Gravit* 43: 1197–1202. https://doi.org/10.1007/s10714-010-0958-8
7. Almarzooqi AM, Maalouf M, El-Fouly THM, et al. (2024) A hybrid machine-learning model for solar irradiance forecasting. *Clean Energy* 8: 100–110. https://doi.org/10.1093/ce/zkad075
8. Jamil B, Irshad K, Algahtani A, et al. (2019) On the calibration and applicability of global solar radiation models based on temperature extremities in India. *Environ Prog Sustainable Energy* 39: e13236. https://doi.org/10.1002/ep.13236
9. Saud S, Jamil B, Upadhyay Y, et al. (2020) Performance improvement of empirical models for estimation of global solar radiation in India: A k-fold cross-validation approach. *Sustainable Energy Technol Assess* 40: 100768. https://doi.org/10.1016/j.seta.2020.100768
10. Sivarajan S, Sundarsingh Jebaseelan SD (2025) A hybrid CNN-RNN based energy consumption forecasting for smart grids in Industries. *Int J Renewable Energy Res* 15: 172–180. https://doi.org/10.20508/ijrer.v15i1.14176.g9031
11. Kushwaha V, Pindoriya NM (2017) Very short-term solar PV generation forecast using SARIMA model: A case study. In *2017 7th International Conference on Power Systems (ICPS)*, Pune, India, 430–435. https://doi.org/10.1109/ICPES.2017.8387332
12. Kumari S, Muthulakshmi P (2023) SARIMA model: An efficient machine learning technique for weather forecasting. *Procedia Comput Sci* 235: 656–670. https://doi.org/10.1016/j.procs.2024.04.064
13. Barus DH, Dalimi R (2021) Determining optimal operating reserves toward wind power penetration in Indonesia based on hybrid artificial intelligence. *IEEE Access* 9: 165173–165183. https://doi.org/10.1109/ACCESS.2021.3135261
14. Alharbi FR, Csala D (2022) A seasonal autoregressive integrated moving average with exogenous factors (SARIMAX) forecasting model-based time series approach. *Inventions* 7: 94. https://doi.org/10.3390/inventions7040094
15. Neshat M, Nezhad MM, Mirjalili S, et al. (2023) Short-term solar radiation forecasting using hybrid deep residual learning and gated LSTM recurrent network with differential covariance matrix adaptation evolution strategy. *Energy* 278: 127701. https://doi.org/10.1016/j.energy.2023.127701

16. Gufron A, Garniwa PMP, Putera DA, et al. (2025) A preliminary LSTM-IDW model for spatiotemporal hourly solar radiation estimation in tropical regions. *Renewable Sustainable Energy Trans* 7: 100105. https://doi.org/10.1016/j.rset.2025.100105
17. Tatachar AV (2021) Comparative assessment of regression models based on model evaluation metrics. *Int Res J Eng Technol* 8: 853–860. Available from: https://www.irjet.net/archives/V8/i9/IRJET-V8I9127.pdf.
18. Ge Y, Nan Y, Bai L (2019) A hybrid prediction model for solar radiation based on long short-term memory, empirical mode decomposition, and solar profiles for energy harvesting wireless sensor networks. *Energies* 12: 4762. https://doi.org/10.3390/en12244762
19. Wang Y, Yao Y, Zou Q, et al. (2024) Forecasting a short-term photovoltaic power model based on improved snake optimization, convolutional neural network, and bidirectional long short-term memory network. *Sensors* 24: 3897. https://doi.org/10.3390/s24123897
20. Sarmas E, Spiliotis E, Stamatopoulos E, et al. (2023) Short-term photovoltaic power forecasting using meta-learning and numerical weather prediction independent long short-term memory models. *Renewable Energy* 216: 118997. https://doi.org/10.1016/j.renene.2023.118997
21. Fang X, Han S, Li J. et al. (2023) A FCM-XGBoost-GRU model for short-term photovoltaic power forecasting based on weather classification. In *2023 5th Asia Energy and Electrical Engineering Symposium (AEEES)*, Chengdu, China, 1444–1449. https://doi.org/10.1109/AEEES56888.2023.10114292
22. Sianturi YCU (2018) Estimating the solar energy potential over Indonesia region using daily sunshine duration. *Int J Sci Res* 9: 1069–1073. https://doi.org/10.21275/SR20510190145
23. Sarjiya, Putranto LM, Irnawan R, et al. (2022) Assessing potential scenarios for achieving new and renewable energy targets in Java-Bali power system, Indonesia. *Int J Energy Econ Policy* 12: 502–515. https://doi.org/10.32479/ijeep.12852
24. Ali H, Sudiarto B, Jufri FH, et al. (2024) Study of reducing transmission losses in Java-Bali system with the addition of capacitors along with optimal capacitor placement methods using quasi-dynamic simulation. *Int J Electr Comput Biomed Eng* 2: 1–18. https://doi.org/10.62146/ijecbe.v2i1.39
25. Rencana Usaha Penyediaan Tenaga Listrik (RUPTL) PT PLN (Persero) 2021–2030. Rencana Usaha Penyediaan Tenaga Listrik 2021–2030, 2019–2028. Available from: https://web.pln.co.id/stakeholder/ruptl.
26. Institute for Essential Services Reform (IESR) (2020) Indonesia Energy Transition Outlook 2025. Essential Concepts of Global Environmental Governance, 86–88. Available from: https://iesr.or.id/en/pustaka/indonesia-energy-transition-outlook-ieto-2025/.
27. Wisudawati N, Fijra R (2021) Analisis Efektivitas Penggunaan Energi Baru Dan Terbarukan Di Provinsi Sumatera Selatan Guna Mendukung REUN 2025. *Integrasi : Jurnal Ilmiah Teknik Industri* 6: 1–9. https://doi.org/10.32502/js.v6i1.3789
28. Saifurrohman MH, Hasyid MH, Putranto LM, et al. (2023) Battery energy storage systems reinforcement control strategy to enhanced the maximum integration of PV to generation systems. *Results Eng* 18: 101184. https://doi.org/10.1016/j.rineng.2023.101184
29. PT PLN Energi Primer Indonesia (2023) Statistics Report 2023. Available from: https://cmsadmin.plnepi.co.id/storage/media/EPI-STATISTIK-2023-1709%20-%20Final%20Cetak.pdf.
30. Mohi Ud Din A, Gupta V (2023) Forecasting and prediction of solar energy in solar photovoltaic plants. *Tuijin Jishu J Propuls Technol* 44: 1457–1469. https://doi.org/10.52783/tjjpt.v44.i4.1080

31. Barhmi K, Heynen C, Golroodbari S, et al. (2024) A review of solar forecasting techniques and the role of artificial intelligence. *Solar* 4: 99–135. https://doi.org/10.3390/solar4010005
32. Zheng K, Sun Z, Song Y, et al., (2025) Stochastic scenario generation methods for uncertainty in wind and photovoltaic power outputs: A comprehensive review. *Energies* 18: 503. https://doi.org/10.3390/en18030503
33. Fang T, Lahdelma R (2916) Evaluation of a multiple linear regression model and SARIMA model in forecasting heat demand for district heating system. *Appl Energy* 179: 544–552. https://doi.org/10.1016/j.apenergy.2016.06.133
34. Nur Aziza V, Moh'd FH, Maghfiroh FA, et al. (2023) Performance comparison of sarima intervention and prophet models for forecasting the number of airline passenger at Soekarno-Hatta International Airport. *BAREKENG J Math Appl* 17: 2107–2120. https://doi.org/10.30598/barekengvol17iss4pp2107-2120
35. Hassani H, Mashhad LM, Royer-Carenzi M, et al. (2025) White noise and its misapplications: Impacts on time series model adequacy and forecasting. *Forecasting* 7: 8. https://doi.org/10.3390/forecast7010008
36. Hassani H, Marvian L, Yarmohammadi M, et al. (2024) Unraveling time series dynamics: Evaluating partial autocorrelation function distribution and its implications. *Math Comput Appl* 29: 58. https://doi.org/10.3390/mca29040058
37. Sghir A, Iroshan A (2024) Unleashing the power of LSTMs: Advancements and applications in sequential data processing, 1–15. https://dx.doi.org/10.2139/ssrn.5032045
38. Kong Y, Wang Z, Nie Y, et al. (2024) Unlocking the power of LSTM for long term time series forecasting. Preprint: https://doi.org/10.48550/arXiv.2408.10006
39. Bousnguar H, Nadji L, Battou A (2023) Gated recurrent units (GRU) for time series forecasting in higher education. *Int J Eng Res Technol* 12: 152–154. Available from: https://www.ijert.org/research/gated-recurrent-units-gru-for-time-series-forecasting-in-higher-education-IJERTV12IS030091.pdf.
40. Wang X, Xu J, Shi W, et al. (2019) OGRU: An optimized gated recurrent unit neural network. *J Phys Conf Ser* 1325: 012089. https://doi.org/10.1088/1742-6596/1325/1/012089
41. Kong X, Chen Z, Liu W, et al. (2025) Deep learning for time series forecasting: A survey. *Int J Mach Learn Cyber* 16: 5079–5112. https://doi.org/10.1007/s13042-025-02560-w
42. Wu YK, Chen CR, Abdul Rahman H (2014) A novel hybrid model for short-term forecasting in PV power generation. *Int J Photoenergy* 2014: 569249. https://doi.org/10.1155/2014/569249

AIMS Press